Journal of Cerebral Blood Flow & Metabolism (2013) 33, 1806–1814

www.jcbfm.com

ORIGINAL ARTICLE

Measuring $\alpha4\beta2$* nicotinic acetylcholine receptor density *in vivo* with [^{18}F]nifene PET in the nonhuman primate

Ansel T Hillmer[1,2], Dustin W Wooten[1,2], Maxim S Slesarev[2], Elizabeth O Ahlers[2], Todd E Barnhart[1], Mary L Schneider[3], Jogeshwar Mukherjee[4] and Bradley T Christian[1,2,5]

[^{18}F]Nifene is an agonist PET radioligand developed to image $\alpha4\beta2$* nicotinic acetylcholine receptors (nAChRs). This work aims to quantify the receptor density (B_{max}) of $\alpha4\beta2$* nAChRs and the *in vivo* (apparent) dissociation constant (K_{Dapp}) of [^{18}F]nifene. Multiple-injection [^{18}F]nifene experiments with varying cold nifene masses were conducted on four rhesus monkeys with a microPET P4 scanner. Compartment modeling techniques were used to estimate regional B_{max} values and a global value of K_{Dapp}. The fast kinetic properties of [^{18}F]nifene also permitted alternative estimates of B_{max} and K_{Dapp} at transient equilibrium with the same experimental data using Scatchard-like methodologies. Averaged across subjects, the compartment modeling analysis yielded B_{max} values of 4.8 ± 1.4, 4.3 ± 1.0, 1.2 ± 0.4, and 1.2 ± 0.3 pmol/mL in the regions of antereoventral thalamus, lateral geniculate, frontal cortex, and subiculum, respectively. The K_{Dapp} of nifene was 2.4 ± 0.3 pmol/mL. The Scatchard analysis based on graphical evaluation of the data after transient equilibrium yielded B_{max} estimations comparable to the modeling results with a positive bias of 28%. These findings show the utility of [^{18}F]nifene for measuring $\alpha4\beta2$* nAChR B_{max} *in vivo* in the rhesus monkey with a single PET experiment.

Journal of Cerebral Blood Flow & Metabolism (2013) **33,** 1806–1814; doi:10.1038/jcbfm.2013.136; published online 14 August 2013

Keywords: B_{max}; K_D; multiple injection; nicotinic acetylcholine receptor; [^{18}F]nifene; PET

INTRODUCTION

Nicotinic acetylcholine receptors (nAChRs) are pentameric ligand-gated ion channels distributed throughout the central nervous system. The $\alpha4\beta2$ subtype is the most abundant subtype of this receptor system. Abnormal $\alpha4\beta2$ nAChR pathologies have been associated with a variety of neuropsychiatric processes and diseases, including neurodevelopmental deficiencies and substance abuse. Reductions in $\alpha4\beta2$ nAChR binding have been found in patients with autism,[1] Parkinson's disease,[2] Alzheimer's disease,[3] and depressive disorder,[4] whereas increased $\alpha4\beta2$ nAChR binding was observed in abstaining smokers.[5]

Quantitative binding metrics such as the binding potential based on nondisplaceable uptake (BP_{ND}) depend on both receptor density (B_{max}) and *in vivo* (apparent) ligand-receptor affinity ($1/K_{Dapp}$).[6] In the case of Alzheimer's disease, Sihver and co-workers[7] used *in vitro* procedures to find that reductions in $\alpha4\beta2$* nAChR binding resulted from decreases in B_{max}. Conversely, lower *in vivo* radiotracer uptake levels found in patients with major depressive disorder analyzed in conjunction with *in vitro* data determined the *in vivo* binding reductions to result from greater concentrations of extracellular acetylcholine, which would increase K_{Dapp}.[4] The ability to perform purely *in vivo* measurements of B_{max} and K_{Dapp} would provide a vastly improved understanding of longitudinal changes to $\alpha4\beta2$* nAChRs and synaptic acetylcholine levels related to neuropathologies.

Regional measurements throughout the brain of $\alpha4\beta2$* nAChR B_{max} have been made with different radioligands in a variety of species. The notation $\alpha4\beta2$* denotes small amounts of binding to other nAChR subtypes that include the $\alpha4$ or $\beta2$ subunits. Reported B_{max} values observed with *in vitro* techniques include experiments with 5-[^{125}I]IA-85380 in humans[8] and [^{3}H]epibatidine in rats.[9] A variety of tritiated ligands were also used for this measurement in the cortex of postmortem human tissue.[10] Each of these studies found the largest receptor density to be present in the thalamus, particularly the lateral geniculate nucleus and antereoprincipal thalamic nucleus. Experiments were also performed using 2-[^{18}F]FA-85380 (2-[^{18}F]FA) to measure B_{max} *in vivo* with the PET multiple-injection (MI) approach in baboons.[11]

In vivo B_{max} measurements with 2-[^{18}F]FA are hindered by slow kinetics, resulting in scanning protocols lasting 270 minutes.[11] [^{18}F]Nifene is an analog radioligand of 2-[^{18}F]FA with faster kinetic properties, as [^{18}F]nifene attains transient equilibrium in the thalamus within 30 minutes while maintaining elevated binding consistent with $\alpha4\beta2$* nAChR distribution in the rhesus monkey brain.[12,13] Further experiments showed rapid displacement of [^{18}F]nifene by nicotine.[14] The fast displacement of [^{18}F]nifene by competing ligands indicates possible sensitivity to acetylcholinesterase inhibitors, a desirable yet elusive trait of PET $\alpha4\beta2$* nAChR radioligands. These kinetic properties of [^{18}F]nifene make it a promising candidate to interrogate the

[1]Department of Medical Physics, University of Wisconsin-Madison, Madison, Wisconsin, USA; [2]Waisman Laboratory for Brain Imaging and Behavior, University of Wisconsin-Madison, Madison, Wisconsin, USA; [3]Department of Kinesiology, University of Wisconsin-Madison, Madison, Wisconsin, USA; [4]Department of Radiological Sciences, University of California-Irvine, Irvine, California, USA and [5]Department of Psychiatry, University of Wisconsin-Madison, Madison, Wisconsin, USA. Correspondence: AT Hillmer, Department of Medical Physics, University of Wisconsin-Madison, 1111 Highland Avenue, Madison, WI 53705, USA.
E-mail: ahillmer@wisc.edu
This work was supported by the following NIH Grants: AA017706, AA10079, AG029479, CA142188, P30-HD03352, and T32-CA009206.
Received 4 March 2013; revised 7 June 2013; accepted 5 July 2013; published online 14 August 2013

$\alpha4\beta2$* nAChR system *in vivo* with simplified experimental protocols.

The aims of this work were, first, to exploit the fast kinetic properties of [^{18}F]nifene and develop an optimized MI experimental design to measure $\alpha4\beta2$* nAChR B_{max} *in vivo* in the rhesus monkey model with PET. The experiments were analyzed with compartment modeling to provide B_{max} and K_{Dapp} measurements. As the optimal MI experimental design provided transient equilibrium of three [^{18}F]nifene injections at varying specific activities, B_{max} was also evaluated with a Scatchard-based analysis method. An additional aim was to evaluate the different analysis methods to provide a comparison of the methods for accurate B_{max} evaluation while considering experimental complexity. Ultimately, quantification of $\alpha4\beta2$* nAChR B_{max} and the K_{Dapp} of [^{18}F]nifene would allow for the development of sensitive experiments to detect small changes to the $\alpha4\beta2$* nAChR system for applications involving disease models or pharmacological intervention.

MATERIALS AND METHODS

Radiochemistry

The production of [^{18}F]nifene was performed following previously published methods.[13] Briefly, nucleophilic substitution of the nitro precursor with [^{18}F]fluoride was performed, followed by purification of the *N*-boc-[^{18}F]nifene intermediate with high-performance liquid chromatography. The intermediate was then deprotected with hydrochloric acid. The final product was pH balanced to 7.0 with sodium bicarbonate and diluted to a 10 mL volume for final formulation. Overall batch yields ranged from 0.9 to 2.4 GBq, whereas specific activities at the time of first injection were 150 to 550 GBq/μmol. Both the nitro precursor and standard compound were purchased from ABX (Radeberg, Germany). Stock solution of nifene standard with a concentration of 0.1 nmol/μL was prepared for MI studies.

Experimental Design

The D-optimal criterion, described in detail by Salinas and co-workers,[15] was used to maximize the identification and precision of the kinetic parameters B_{max}, k_{on}, and k_{off} to select the optimal MI experimental design. Optimization of MI experiments focused on the thalamic regions of the brain. As the true parameter values were not known *a priori*, initial parameter estimates ranged from 0.01 to 0.5 mL/pmol per min for k_{on} and 0.05 to 0.5 1/min for k_{off}, with K_{Dapp} constrained to vary between 1.0 and 4.0 pmol/mL. B_{max} ranged from 1.0 to 6.0 pmol/mL, consistent with literature values for thalamic $\alpha4\beta2$* nAChR densities.[8,9,11] Candidate protocols included both two- and three-injection schemes and varied both the specific activity and the injection times. Arterial input functions from our previous work[13] were used for the optimizations, which were performed with COMKAT software.[16]

PET Experiment Data Acquisition

PET data were acquired on a Concorde microPET P4 scanner, which has a 7.8-cm axial field of view, 19-cm transaxial field of view, and a reported in-plane spatial resolution of 1.75 mm.[17] The actual spatial resolution was 2.80 mm in reconstructed images using the experimental conditions and processing methods reported herein. Scans were performed on a total of four *Macaca mulatta* (rhesus monkey) subjects (3 female, 1 male; 6.1 to 11.9 kg; 4.6 to 12.9 years; subject names: RH1: BD66; RH2: BD22; RH3: BD67; RH4: AY96). Three subjects received experiments consisting of three [^{18}F]nifene injections (RH1, RH2, and RH3), whereas another experiment was included with two [^{18}F]nifene injections (RH4). Subjects were anesthetized before PET procedures with 10 mg/kg ketamine (intramuscularly), and maintained on 1% to 1.5% isoflurane throughout the experiment. Atropine sulfate was given to minimize secretions. Once anesthetized, the subject was placed in a stereotaxic headholder, and a 518 second transmission scan was acquired with a ^{57}Co point source. Emission data acquisition was initiated simultaneously with a fast bolus injection of tracer dose [^{18}F]nifene and continued for 105 to 120 minutes. Heart rate, breathing rate, body temperature, and SpO_2 (blood oxygen saturation) levels were monitored throughout the procedure. On experiment completion, the subject was returned to its cage and monitored until fully alert. All housing and experimental guidelines were approved by the institutional animal care and use committee (IACUC). These procedures are in accordance with the stringent regulations encompassing the ethical care and use of laboratory animals, as published in the USDA 'Federal Register' standards, and the 'Guide for the Care and Use of Laboratory Animals' set forth by the NIH (Bethesda, MD, USA).

Measurement of [^{18}F]Nifene in the Blood

Parent [^{18}F]nifene in the blood was measured to provide a parent input function for kinetic modeling. Arterial blood samples were withdrawn throughout all PET scans, starting with rapid sampling immediately after a bolus injection of [^{18}F]nifene and slowing to 10 minute sampling at late time points. Radioactivity measurements of the whole blood, plasma, and denatured plasma were made with a 2-inch NaI(Tl) well counter cross-calibrated with the PET scanner following our lab's previous published methods.[13] The hematocrit was also measured to correct for the heparinized saline present in the final extract volume. Select samples were used for thin layer chromatography analysis to generate a unique metabolite correction for each subject as described previously.[13]

The implementation of the MI compartment model in COMKAT requires the definition of a distinct input function for each injection. To separate the radioactivity from each radioligand injection present in the plasma, the radioactivity concentration curves (before metabolite correction) from 20 minutes after injection until the following injection were fit to decaying exponential functions. Fitting procedures were constrained such that the late decay constant was uniform across all injections for each subject. The resulting fit functions were extrapolated to the end of the study and subtracted from all subsequent injections to generate separate input functions for each injection. The same metabolite correction was then applied to each injection curve to obtain parent [^{18}F]nifene input data expressed as radioactivity (Bq/cm^3). The metabolite-corrected radioactivity curve was divided by the specific activity expressed as a function of time to yield an input function (C_P) in units of nifene molar concentration (pmol/cm^3), independent of radioactive decay. Finally, the observed plasma data were fit to the following analytic function:[18]

$$C_P(t) = (c_0(t-\tau) - c_1)e^{-\gamma_1(t-\tau)} + c_2e^{-\gamma_2(t-\tau)} + c_3e^{-\gamma_3(t-\tau)} + c_4e^{-\gamma_4(t-\tau)} \quad (1)$$

where γ_i represents the different elimination rates of radioligand from the arterial plasma.

PET Image Processing

Dynamic PET data were histogrammed from list mode into time frames of 8×30 seconds, 6×1 minutes, followed by 2 minute frames until 2 minutes before a subsequent injection, with 30 second frames for the remainder of the injection. This binning scheme was repeated for all injections in the study. Sinograms were reconstructed with filtered back projection using a 0.5 1/cm ramp filter, and included corrections for arc, scatter, attenuation, and scanner normalization. The reconstructed images were subjected to a denoising algorithm[19] using a $3 \times 3 \times 3$ voxel filtering kernel. The processed images had a final matrix size of $128 \times 128 \times 63$ with voxel dimensions of $1.90 \times 1.90 \times 1.21$ mm^3.

Regions of interest were hand drawn with multiple circles on various brain regions. The cerebellum (CB) was defined on early summed images, taking care to focus on grey matter and exclude the vermis region, with a resulting volume of 663 mm^3. Regions of elevated binding were drawn on late summed images based on areas of high radiotracer uptake. The thalamus was subdivided into the general regions of the antereoventral thalamus (AVT) and lateral geniculate body (LG), with respective volumes of 231 and 161 mm^3. The frontal cortex (FC) and subiculum (SB), a substructure of the hippocampus, were identified as regions of moderate uptake, and contained volumes of 763 and 314 mm^3. These regions are shown in Figure 1. Time–activity curves were extracted from these five regions for analysis.

Parameter Estimation: Compartment Modeling

The model constructed for experimental design and analysis was based on the two-tissue compartment model. The first compartment in the tissue is the free compartment ($F(t)$), which includes both free and nonspecifically bound ligand. The second tissue compartment is the specifically bound compartment ($B(t)$). The amount of ligand in $B(t)$ has a maximum concentration, B_{max} (pmol/mL), the receptor density.[20] The radioligand concentration in the plasma ($C_P(t)$) is experimentally measured. Ligand

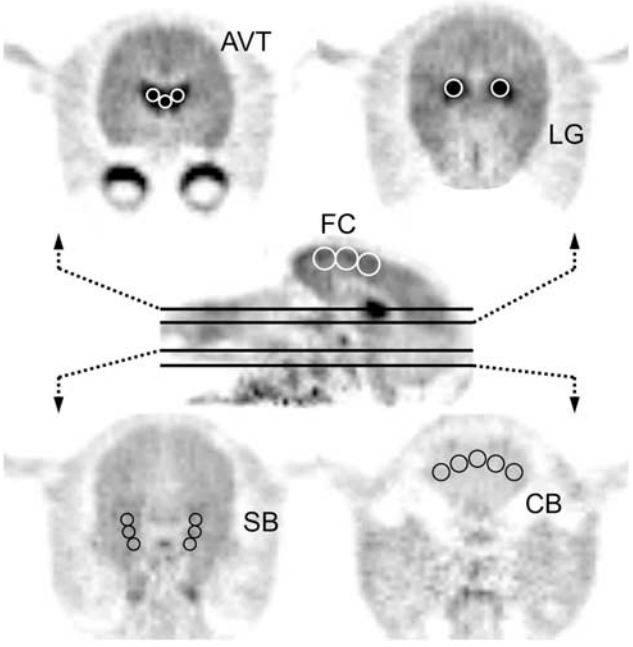

Figure 1. Regions of interest identified on PET images summed from 20 to 45 minutes. These regions include the antereoventral thalamus (AVT), lateral geniculate (LG), frontal cortex (FC), subiculum (SB), and cerebellar gray matter (CB). The middle sagittal image showing the FC is taken midbrain, and the planes of the transaxial images are indicated with black lines.

transfer between these compartments and the plasma is described by the differential equations

$$\frac{dF_i(t)}{dt} = K_1 C_{Pi}(t) - k_2 F_i(t) - k_{on} F_i(t)\left[B_{max} - \sum_i B_i(t)\right] + k_{off} B_i(t) \quad (2)$$

$$\frac{dB_i(t)}{dt} = k_{on} F_i(t)\left[B_{max} - \sum_i B_i(t)\right] - k_{off} B_i(t) \quad (3)$$

The rate constants K_1 (mL/mL per min) and k_2 (1/min) parameterize the transport of ligand from the plasma to the tissue and tissue clearance, respectively. The parameters k_{on} (mL/pmol per min) and k_{off} (1/min) represent ligand binding to the receptor site and dissociation in the *in vivo* setting. The implementation of MI studies requires unique $B(t)$ and $F(t)$ compartments for each injection. Therefore, a unique set of the above equations is required to describe the ith injection.[21]

The modeled PET signal for frame j, C_{PETj}, includes radioactivity from both the $B(t)$ and $F(t)$ compartments at time t summed over all injections, and is expressed as follows:

$$C_{PETj} = \frac{1}{t_j - t_{j-1}} \int_{t_{j-1}}^{t_j} dt \sum_i sa_i(t)(1 - f_V)(F_i(t) + B_i(t)) + f_V A_i(t) \quad (4)$$

The constant f_V represents the fractional blood volume accounting for the signal from the whole blood measured in the vasculature ($A_i(t)$), and was set to $f_V = 0.04$. Model implementation requires ligand concentrations in units of molar concentrations (pmol/mL); therefore, the specific activity term $sa_i(t)$ converts the model concentrations in $F_i(t)$ and $B_i(t)$ to nondecay-corrected radioactivity units of Bq/cm^3.

Parameters were estimated by minimizing the residual sum of squares between the modeled PET signal and the observed PET signal (*PET*). The Levenberg–Marquardt optimization algorithm was used to perform this minimization with the following objective function:

$$o(p) = \sum_{r=1}^{R} \sum_{j=1}^{J} w_{r,j}(PET_{r,j} - C_{PETr,j})^2 \quad (5)$$

The objective function was optimized over J PET frames for given parameters p, where $p \subseteq P = \{k_{on}, k_{off}, V_{ND}, (K_1)_R, (B_{max})_{R-1}\}$ over $R = 5$ regions. The parameters included in p depended on the step in the fitting procedure (see below). The weighting factor of each PET frame was determined from the time duration by $w_{r,j} = (t_j - t_{j-1})$, and included no contribution from the measured PET data.[22] Model implementation and parameter estimation were performed with COMKAT software.[16] A more in-depth description of the implementation of equations (2)–(5) has been detailed elsewhere.[21]

The following assumptions were made to improve parameter identifiability across brain regions:

(1) The nondisplaceable distribution volume ($V_{ND} = K_1/k_2$) was assumed uniform and unchanging throughout all brain regions. K_1 was allowed to vary across regions to account for regional differences in blood flow, but did not vary over time throughout the experiment.
(2) The CB was assumed to contain negligible specific binding, consistent with previous findings examining [^{18}F]nifene in the rhesus monkey.[14] Therefore, CB data were modeled without specific binding compartments ($B(t)$).
(3) The ligand binding and dissociation parameters, k_{on} and k_{off}, were assumed uniform across all regions of specific binding.

These assumptions were implemented in the following three steps:

Step 1: The CB, a region of negligible [^{18}F]nifene binding, was analyzed using a model which omitted $B(t)$ to determine V_{ND} for subsequent analysis of specific binding regions. The objective function in this step was optimized for $p = \{K_1, V_{ND}\}$

Step 2: The high uptake regions of the AVT and LG were analyzed using the fixed V_{ND} value found in Step 1 to obtain estimates of the global parameters k_{on} and k_{off}, as well as the regional parameters K_1 and B_{max}. The objective function was therefore optimized for $p = \{k_{on}, k_{off}, (K_1)_r, (B_{max})_r\}$, where $r = 2$.

Step 3: The k_{on}, k_{off}, and V_{ND} values found in previous steps were fixed to determine K_1 and B_{max} in the FC and SB regions. The objective function was optimized for $p = \{(K_1)_r (B_{max})_r\}$, where $r = 2$.

Uncertainties in parameter estimates were examined with Monte Carlo methods as reported previously.[15,23] The optimized parameters for each study were used to simulate noise-free data. Simulated noise was then introduced according to the equation

$$C_{noise} = C_{fit} + \left(N_{(0,1)} c_1 \sqrt{C_{fit}} + N_{(0,1)} c_2\right) \quad (6)$$

where C_{noise} is the simulated time–activity curve with added noise, C_{fit} is the noise-free simulated time–activity curve, $N_{(0,1)}$ is a random number generated from a normal distribution with $\mu = 0$ and $\sigma = 1$, and c_1 and c_2 are scaling factors to obtain noise levels similar to the experimentally observed time–activity curves ($10 < c_1 < 40$, $100 < c_2 < 500$). A total of 100 noisy simulated data sets for each subject were constructed and the parameters were estimated. The coefficient of variation ($cov = s.d./mean \times 100\%$) was measured for each parameter for each subject and recorded.

Parameter Estimation: Scatchard Analysis

Analysis of the PET data included an alternative methodology to measure B_{max} and K_{Dapp} *in vivo* with PET using a Scatchard-type analysis, which requires equilibrium at the receptor site.[24] As [^{18}F]nifene rapidly establishes transient equilibrium, B_{max} and K_{Dapp} measurements were performed with this method to compare with compartment modeling techniques. Based on previous linearized Scatchard methodologies,[25] the present work evaluated (B/F) at transient equilibrium to regionally estimate B_{max} and K_{Dapp} with the following linearized form of the Scatchard plot:

$$\frac{B}{F} = \frac{B_{max}}{K_{Dapp}} - \frac{1}{K_{Dapp}}\left(\frac{B}{F}\right)F \quad (7)$$

To determine when transient equilibrium occurred, the parameters resulting from compartment modeling analysis were used to model $B(t)$ and $F(t)$ throughout the experiment. The PET frames when $dB(t)/dt = 0$, indicating transient equilibrium, were used for Scatchard analysis. PET time–activity curves were 'denoised' by fitting data from 15 minutes after injection to the end of each injection to a decaying exponential function. The total PET signal from the CB was then separated into contributions from each individual [^{18}F]nifene injection by extrapolating the resulting CB fits to the end of the scan and subtracting the extrapolated fits from all subsequent injections. The residual-free CB value for each injection was

determined at transient equilibrium and recorded as CB_i for the ith injection. The free radioligand concentration F_i was calculated as

$$F_i = \sum_j^i \frac{CB_j}{SA_j},$$

where SA_i is the decay-corrected specific activity of the ith injection. The specific binding fit at transient equilbrium was recorded as S_i. The ratio B/F_i was evaluated as

$$\left(\frac{B}{F}\right)_i = \frac{S_i}{\sum_j^i CB_j} - 1.$$

The x-value,

$$\left(\frac{B}{F}F\right)_i = \left(\frac{S_i}{\sum_j^i CB_j} - 1\right) \times \sum_j^i \frac{CB_j}{SA_j},$$

was plotted against the y-value,

$$\left(\frac{B}{F}\right)_i = \frac{S_i}{\sum_j^i CB_j} - 1.$$

Linear least-squares fitting was performed on the linearized Scatchard data to determine the slope m and y-intercept y_0 of the plot. B_{max} and K_{Dapp} were estimated as $B_{max} = y_0 K_{Dapp}$ and $K_{Dapp} = -1/m$, respectively. The uncertainties of these parameters were determined exclusively based on the regression analysis. This Scatchard analysis was only performed in experiments with three injections of [^{18}F]nifene data (RH1–RH3).

RESULTS

Optimization of Experimental Design

Optimization of MI experimental design revealed that identification of specific binding parameters was most sensitive to the nifene dose in the second injection. A dosage of 0.8 to 2.0 nmol/kg nifene (approximately 70% to 75% receptor occupancy) administered in the second injection optimally determined B_{max}, k_{on}, and k_{off} (see Figure 2A). The duration of data acquisition beyond 30 minutes for any injection did not improve parameter identification. Uncoupling of B_{max} and k_{on} with the optimal experiment design is shown by the sensitivity functions illustrated in Figure 2B. The resulting experimental protocols used for the four experiments presented herein are detailed in Table 1.

Compartment Modeling Measurements of B_{max} and [^{18}F]Nifene Kinetic Parameters

All input functions were analytically defined by fitting the blood data to equation (1). When radioligand was given as a slow bolus (30 to 60 seconds) for injections with a greater cold nifene mass, the third exponential term overparameterized the data ($c_4 = 0$). A sample fit is displayed in Figure 3 (top). No deviations to the subject's physiologic parameters were observed following the administration of high nifene masses.

Parameter estimates obtained with compartment modeling are listed in Table 2. High identifiability of B_{max} was found in the high binding thalamic regions, where average B_{max} values of 4.8 ± 1.4 and 4.3 ± 1.0 pmol/mL were measured in the AVT and LG, respectively. The parameters k_{on} and k_{off} could not be sufficiently uncoupled, as the correlation coefficient ($\rho_{k_{on},k_{off}}$) between the two parameters was >0.93 for all experiments. Therefore, measurements of the composite parameter $K_{Dapp} = k_{off}/k_{on}$ are presented. The average value of K_{Dapp} was 2.4 ± 0.3 pmol/mL. In the moderate receptor density regions of the FC and SB, average B_{max} values of 1.2 ± 0.4 and 1.2 ± 0.3 pmol/mL were observed. The uncertainty of each parameter estimate was estimated with Monte Carlo methods. These simulations found the highest variability in the B_{max} parameters ($cov = 12\%$ to 15% for all regions) and K_{Dapp} ($cov = 18\%$). Sample fits of the measured PET time course for three regions (CB, AVT, and SB) are included in Figure 3.

The sensitivity curves in Figure 2B showed little parameter uncoupling during the third injection. Therefore, compartment modeling parameter and uncertainty analysis was performed on the first two injections of data from experiments with three injections. A comparison of the resulting values from the two injection and three injection analyses yielded estimations of B_{max} and K_{Dapp} within 1σ of the values determined with the full scan of data. No significant bias was apparent in the thalamic specific binding parameters (Figure 5B).

Table 1. Experiment protocols

Injection	*What*	*RH1*	*RH2*	*RH3*	*RH4*
	Subject mass (kg)	6.1	7.6	7.3	6.7
	Subject sex	F	F	M	F
	Time (min)	0	0	0	0
1	Activity (MBq)	94	83	85	126
	Mass (nmol)	0.2	0.1	0.1	0.6
	Time (min)	45	45	45	60
2	Activity (MBq)	103	77	75	124
	Mass (nmol)	14	10	11	18
	Time (min)	91	90	90	—
3	Activity (MBq)	91	69	74	—
	Mass (nmol)	106	46	42	—

F, female; M, male.

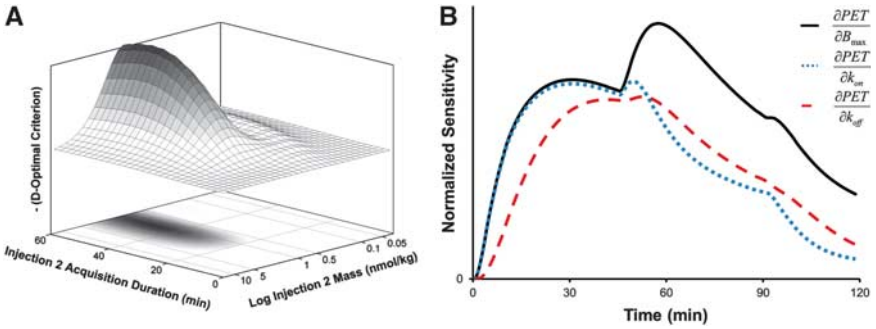

Figure 2. Development of multiple-injection (MI) experimental design. (**A**) Illustrates the dependence of the D-optimal criterion on the administered nifene mass and time duration for the second injection. (**B**) The normalized sensitivity curves for k_{off} (dashed), k_{on} (dotted), and B_{max} (solid) for the optimal design used with experiments RH2 and RH3 in the thalamus.

Scatchard Measurements of B_{max} and K_{Dapp}

Modeling of the kinetic parameters resulting from the MI analysis determined that transient equilibrium was established within 35 minutes after injection for all injections. Measurements of B_{max} and K_{Dapp} with Scatchard plots are shown in Figure 4. Using uncertainties from the linear fit, *cov* values of 17% to 30% and 14% to 28% were found for B_{max} and K_{Dapp}, respectively, in thalamic regions. Estimates of B_{max} and K_{Dapp} with this graphical analysis are compared with the MI technique, as shown in Figure 5A. As the three-point Scatchard plots tended to exhibit nonlinearity, two-point Scatchard plots were generated for experiments RH1–RH3 in each of the specific binding regions. A slight positive bias in the B_{max} estimations was apparent with the two-point Scatchard plots relative to the values found with the compartment modeling (Figure 5C).

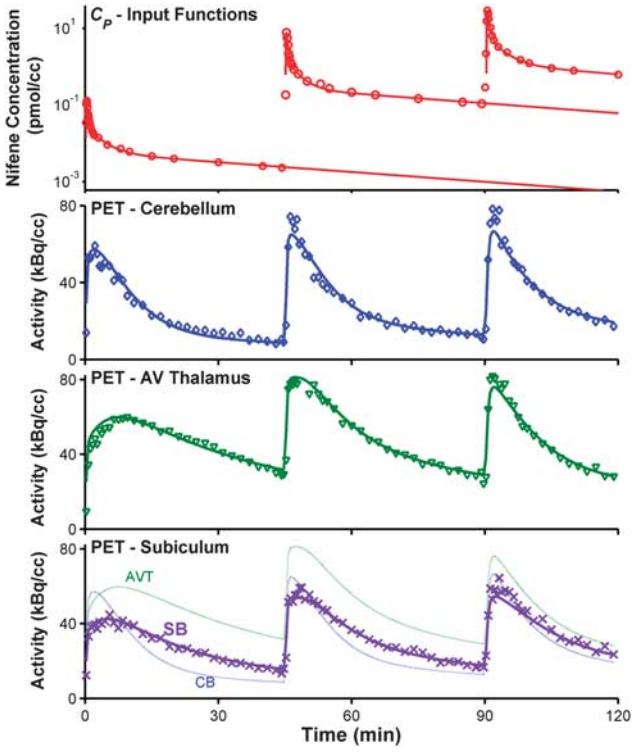

Figure 3. Compartment modeling of [^{18}F]nifene data. The top plot shows the parent input function C_P, with measured blood data (○) and the resulting fit to an analytic function (solid lines) for a sample subject (RH2). The corresponding PET time–activity curves and model fits are shown in the bottom three plots. The observed data are indicated with discrete symbols, whereas the optimized model fit is shown with solid lines. The three regions shown include the negligible binding region of the cerebellum (CB, ◇), the high binding region of the antereoventral thalamus (AVT, ▼), and the moderate binding subiculum region (SB, x). The model fits for all three regions are shown on the bottom plot to provide direct comparison of the PET signal for different levels of specific binding.

DISCUSSION

This work developed experiments that used [^{18}F]nifene to measure directly *in vivo* $\alpha4\beta2$* nAChR receptor density. Compartment modeling of these experiments yielded B_{max} values of 4.8 ± 1.4 pmol/mL in the AVT and 4.3 ± 1.0 pmol/mL in the LG of the rhesus monkey. Extrathalamic B_{max} measurements made assuming the thalamic K_{Dapp} value in cortical regions yielded estimates of 1.2 ± 0.4 pmol/mL in the FC and 1.2 ± 0.3 pmol/mL in the SB. A previous *in vivo* measurement of $\alpha4\beta2$* nAChR B_{max} was made by Gallezot and co-workers,[11] who found values of 3.0 ± 0.4 pmol/mL in the thalamus and 0.6 ± 0.1 pmol/mL in the FC using 2-[^{18}F]FA with MI techniques in baboons. The reported regional *in vitro* assays included values of 1.5 ± 0.6 pmol/g of tissue in the thalamus and 0.45 ± 0.03 pmol/g of tissue in the cingulate cortex with 5-[^{125}I]IA-85380 in humans,[8] and 0.9 pmol/g of tissue measured with [^{3}H]epibatidine in human cerebral cortex.[9] Although these experiments were performed in a variety of species with different methodologies, the similarities within order of magnitude indicate agreement with the B_{max} values presented herein.

A first precise measure of [^{18}F]nifene K_{Dapp}, 2.4 ± 0.3 pmol/mL, is reported. This value compares well with our previous work, which preliminarily estimated a K_{Dapp} of 3 ± 1 pmol/mL for [^{18}F]nifene in the rhesus monkey with a Scatchard-like analysis assuming the same K_{Dapp} across all subjects.[13] The different affinities for nAChR $\alpha4$- and $\beta2$-inclusive subtypes likely influenced the observed K_{Dapp} value. As nifene lacks the sensitivity to differentiate between these subtype affinities, the observed value is likely most representative of [^{18}F]nifene's K_{Dapp} for the $\alpha4\beta2$ subtype because of its high thalamic density relative to other nAChR subtypes. The only other

Table 2. Parameter estimation, compartment modeling (full experiment)

Region	*Parameter (units)*	*RH1*	*RH2*	*RH3*	*RH4*	*M.C. cov*[a] (%)	*Pop. mean*
CB	K_1 (mL/mL per min)	0.83	1.03	0.84	1.14	3	0.96 ± 0.15
	k_2 (1/min)	0.18	0.22	0.17	0.27	3	0.21 ± 0.05
	V_{ND} (unitless)	4.65	4.78	4.91	4.14	2	4.62 ± 0.34
AVT and LG	K_{Dapp} (pmol/mL)	2.14	2.81	2.36	2.23	18	2.39 ± 0.30
AVT	K_1 (mL/mL per min)	0.80	0.89	0.69	1.13	4	0.88 ± 0.19
	B_{max} (pmol/mL)	5.97	5.88	4.31	3.12	13	4.82 ± 1.37
LG	K_1 (mL/mL per min)	0.62	0.80	0.61	0.83	5	0.72 ± 0.12
	B_{max} (pmol/mL)	4.21	5.34	4.56	2.98	15	4.27 ± 0.98
FC	K_1 (ml/mL per min)	0.62	0.88	0.74	0.93	4	0.79 ± 0.14
	B_{max} (pmol/mL)	1.33	1.28	1.62	0.68	14	1.23 ± 0.39
SB	K_1 (mL/mL per min)	0.54	0.74	0.54	0.28	4	0.53 ± 0.19
	B_{max} (pmol/mL)	1.50	1.21	1.23	0.72	12	1.17 ± 0.32

AVT, antereoventral thalamus; CB, cerebellum; FC, frontal cortex; LG, lateral geniculate body; SB, subiculum.
[a]The average coefficient of variation (*cov* = *s.d./mean* × 100%) for parameter estimates determined using Monte Carlo methods.

$\alpha4\beta2$* nAChR radioligand with an *in vivo* K_{Dapp} measurement is 2-[^{18}F]FA, which was found to have a K_DV_R value of 1.3 ± 0.4 pmol/mL.[11] Given the larger BP_{ND} of 2-[^{18}F]FA compared with that of [^{18}F]nifene, a larger K_{Dapp} value would be expected for [^{18}F]nifene assuming both tracers bind to the same receptor sites (i.e., have the same B_{max}).

Analysis with Compartment Modeling

Successful identification of kinetic parameters with MI experiments requires precise experimental design. The D-optimal criterion, which focused on uncoupling B_{max}, k_{on}, and k_{off} in the thalamus, determined the optimal cold ligand dose and injection times. The resulting protocol uncoupled B_{max} from k_{on} and k_{off} with the administration of a nifene dose eliciting a peak transient occupancy of 70% to 75% in the second injection. The optimization results further suggested that a roughly 6 nmol/kg nifene dose (>90% occupancy) given in the third injection would separately identify k_{on} and k_{off}. In practice, however, these parameters were not uncoupled during analysis of the experimental data (as shown in Figure 2B), as initial simulations underestimated k_{on} and k_{off}.

To provide insight into k_{on} and k_{off} values, a family of simulated thalamic PET curves was generated using the measured parameter values from Table 2 while incrementing k_{on} and k_{off} with K_{Dapp} fixed to compare with the observed PET data. This brief analysis revealed that k_{off} values slower than 0.1 1/min significantly reduced the quality of fit, making this a lower bound for k_{off} for this experimental design. In this work, the experiment with the lowest correlation coefficient between k_{on} and k_{off} (RH3, $\rho_{k_{on},k_{off}} = 0.93$) resulted in $k_{off} = 0.32 \pm 0.07$ 1/min and $k_{on} = 0.14 \pm 0.03$ mL/pmol per min, yielding speculative values likely biased by parameter coupling in the fit. For comparison 2-[^{18}F]FA was found to have a k_{off} value of 0.33 ± 0.07 1/min.[11] The fast k_{on} and k_{off} values partially explain the inability to separate the two parameters. The close similarity in k_2 (~0.2 1/min) and k_{off} (>0.1 1/min) also likely contributed to the inability to identify uniquely k_{on} and k_{off}, as the two transfer routes occur at similar rates that the model cannot readily distinguish.

The specific binding parameters B_{max} and k_{on} were coupled to k_2 because of the fast ligand binding and dissociation rates of [^{18}F]nifene. To examine the repercussions of an unconstrained V_{ND} in regions of specific binding, a model was implemented to simultaneously estimate K_1, V_{ND}, B_{max}, and K_{Dapp} exclusively in the AVT and LG. This model configuration yielded an 11% inflation of V_{ND} and reductions in B_{max} (−20%) and K_{Dapp} (−16%). Therefore, to minimize potential parameter coupling between the radioligand delivery and specific binding parameters, V_{ND} was measured in the CB, and subsequently assumed constant throughout the brain by fixing V_{ND} (but not K_1) in regions with specific binding. The assumption of a uniform V_{ND} is commonly made with a reference region graphical analysis techniques.[26] When data exclusively from the CB was modeled to measure separate V_T values for each injection, these values agreed within 6% with no appreciable correlation of V_T with nifene mass, justifying the omission of specific binding in modeling the CB.

The initial model for parameter estimation was constructed to generate unique B_{max}, k_{on}, and k_{off} values for each region; however, high coupling of B_{max} and K_{Dapp} in the cortical regions resulted in unidentifiability of those parameters in the FC and SB ($\rho_{B_{max},k_{on}} > 0.9$). Separate K_{Dapp} values in the AVT and LG were within 10% of each other, suggesting K_{Dapp} may be uniform in the thalamus. The assumption of a uniform K_{Dapp} was extended to the FC and SB to provide preliminary estimations of B_{max} in the cortical regions. A similar approach was used in experiments estimating extrastriatal D2 B_{max} by fixing k_{off} to the value observed in the basal ganglia.[27] Assuming a global K_{Dapp} represents a limitation in the present results, as our group has previously shown regional K_{Dapp} variations in experiments examining the serotonin system with MI techniques.[28] Consequently, the extrathalamic B_{max} estimations may be biased if endogenous concentrations of acetylcholine vary across different brain regions. A different experimental design explicitly optimized for cortical regions is necessary to properly measure B_{max} and K_{Dapp} in the cortex.

Uptake of [^{18}F]nifene into the tissue occurred rapidly, as an average K_1 value of 1.0 ± 0.1 mL/mL per min was observed in the CB with values of 0.8 ± 0.2 mL/mL per min found in both the AVT and LG. These high K_1 values are consistent with complete extraction of radioligand from the plasma to tissue. Previous *in vitro* studies have indicated that transfer of 2-[^{18}F]FA across the blood–brain–barrier (BBB) principally occurs because of free diffusion.[29] Although [^{18}F]nifene ($\log P = -0.5$;[12]) is more lipophilic than 2-[^{18}F]FA ($\log D = -1.5$;[29]), both radioligands exhibit low lipophilicity, which predicts slow diffusion rates across the BBB.[30] The order of magnitude variation in K_1 between the two radioligands, however, suggests the possibility of a transport mechanism to account for the fast uptake rates of [^{18}F]nifene. One possible candidate for this mechanism is the BBB amine transporter.[31] Previous studies have found that another $\alpha4\beta2$* nAChR radioligand, [^{18}F]flubatine (formerly [^{18}F]NCFHEB), also interacts with this transporter.[32] We investigated using a model with separate K_1 parameters for each injection to account for high mass potentially altering transfer rates of [^{18}F]nifene across the BBB. This model reduced parameter identifiability while yielding K_1 estimates that did not correlate with administered nifene mass. Therefore, K_1 was assumed unvarying throughout the entire experiment. The BBB amine transporter is an area of interest for future experiments aimed at improving understanding of the passage of [^{18}F]nifene across the BBB.[33]

As the third injection of data could not uncouple k_{on} and k_{off}, data from only the first two injections of the three injection experiments were analyzed with the same model. This analysis yielded B_{max} and K_{Dapp} values consistent with results from analyzing the full three-injection data set, as shown in Figure 5B. The precision of the two-injection analysis was comparable, with average B_{max} *cov* values of 15%, whereas K_{Dapp} *cov* values were 19%. A slight underestimation of the specific binding parameters was observed with the two-injection analysis; however, the estimates were within 1σ of the three-injection parameter values. Our previous work included two experiments with two-injection [^{18}F]nifene protocols of appropriate mass to provide approximations of B_{max} and K_{Dapp}.[13] One experiment was not included in this work because of different blood sampling methods, whereas the other was included (M2 from ref. 13 corresponds to RH4 here). Modifications to the data processing of this subject (e.g., different regions of interest, input function interpolation) resulted in estimates of BP_{ND} and V_{ND} that are comparable but not identical to previously reported values. This subject (RH4) had the lowest B_{max} value and was also the oldest, with an age of 12.9 years compared with other subjects (4.6 to 5.2 years). Although only four subjects were reported here, this lower receptor density may result from differences in age groups.[34]

Analysis with the Scatchard Method

MI experiments provide measurements of B_{max} in a non-equilibrium setting, which distinguishes this method from Scatchard-like methods requiring equilibrium for successful B_{max} measurements. The optimal MI experimental design for measurement of B_{max} and K_{Dapp} with [^{18}F]nifene, however, included transient equilibrium for each injection because of the fast kinetic properties of this radioligand. Consequently, measurements of B_{max} and K_{Dapp} were also made with a Scatchard methodology to compare directly the compartment modeling method

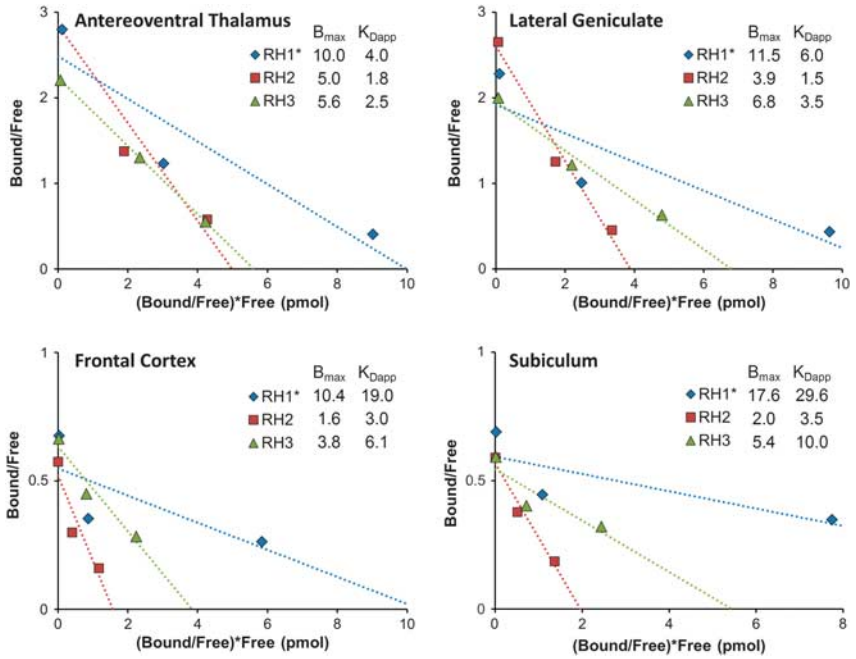

Figure 4. Measurements of B_{max} and K_{Dapp} with a Scatchard-type analysis in four different regions (labeled top left). *Denotes the poor fit in experiment RH1 because of receptor saturation by the high nifene dosage given in the third injection.

with a method that did not require blood sampling. It should be stressed, however, that the selected doses for the present experiments were based on the optimal design for MI (nonequilibrium) analysis rather than Scatchard analysis. Therefore, alternative dosages are likely more appropriate for experiments utilizing a Scatchard analysis.

The resulting Scatchard plots, shown in Figure 4, yielded B_{max} values compatible with compartment modeling results in the thalamic regions in two experiments (RH2 and RH3). Experiment RH1 exhibited a nonlinear trend resulting in overestimations of B_{max} and K_{Dapp}; however, the administered nifene dose in the third injection for this experiment more than doubled the mass given for RH2 and RH3 (see Table 1). We conclude that this dose (17.4 nmol/kg) saturated the receptors and yielded unreliable results. Indeed, the third injection for RH2 and RH3 may have saturated the extrathalamic regions, indicated by the slight nonlinearity in the Scatchard plots and large positive bias in B_{max} compared with compartment modeling methods. A two-point Scatchard analysis, which ignored data from the third near-saturation injection to avoid the resulting nonlinearities, was also performed. Although two-point Scatchard measurements are vulnerable to inaccuracies resulting from fitting two points to a line, this brief analysis estimated B_{max} values in better agreement with those measured with compartment modeling (Figure 5C). Lower nifene dosages, yielding receptor occupancies of roughly 30% to 50% and 70% to 75%, respectively, for each injection, may yield improved B_{max} and K_{Dapp} measurements with the three-point Scatchard analysis method. A bolus-infusion protocol achieving true equilibrium could also improve the accuracy and precision of this method,[25] but at the expense of increased experimental complexity.

It is difficult to compare directly the presented analysis techniques as the experiments were optimized for compartment modeling analysis but not Scatchard analysis. Based on the available data, the two-injection compartment model paradigm provided the best method for measurements of B_{max} and K_{Dapp} with a better combination of experimental simplicity and parameter precision. Reducing the experimental protocol from three injections to two injections lessened the duration of scanning procedures to 90 minutes of data acquisition, and simulations suggest this could be further shortened to 70 minutes. Conversely, accurate estimates of B_{max} and K_{Dapp} with Scatchard analysis would require at least three injections of [^{18}F]nifene and 120 minutes of scanning. The compartment modeling techniques also showed higher parameter precision. Although the fast kinetics of [^{18}F]nifene prevented unique identification of k_{on} and k_{off} with the compartment modeling analysis, this technique yielded excellent identification of B_{max} ($\rho_{B_{max},k_{on}} < 0.3$), giving a high degree of confidence in the presented measurements. Theoretical advantages of MI techniques for measurement of B_{max} and K_{Dapp} are further discussed elsewhere.[21,35]

Applicability to Human Studies

The separate evaluation of $\alpha4\beta2$* nAChR B_{max} and K_{Dapp} is important for human translation for research applications in a variety of complex neuropsychiatric processes. For example, these measurements would improve the understanding of longitudinal changes undergone by acetylcholine receptors, ligand-receptor affinity, and synaptic acetylcholine concentrations in the progression of Alzheimer's disease.[3] Information regarding how receptor density and synaptic acetylcholine are differentially modulated during tobacco exposure and abstinence could lead to improved design of smoking cessation treatments.[5] Similar experiments could also improve understanding and treatment of depressive disorder.[4]

Future toxicological and pharmacological measurements of nifene are needed to determine if nifene doses inducing significant receptor occupancies would be ethical in humans. The 0.6 nmol/kg dose used for the present experiments resulted in $\alpha4\beta2$* nAChR occupancies of roughly 70%; however, saturation of these receptors has been reported with no adverse side effects in 2-[^{18}F]FA smoking studies.[36]

The rhesus monkey appears to be a unique species with negligible $\alpha4\beta2$* binding in the CB, as baboons and humans have

A	3I C.M.	2I C.M.	3I ScA	2I ScA
AVT	5.4±0.9	5.2±0.8	6.9±2.7	4.8±1.2
LG	4.7±0.6	4.2±0.5	7.4±3.8	4.3±1.1
FC	1.4±0.2	1.3±0.2	5.3±4.6	1.7±0.8
SB	1.3±0.2	1.2±0.2	8.2±8.3	2.2±0.8

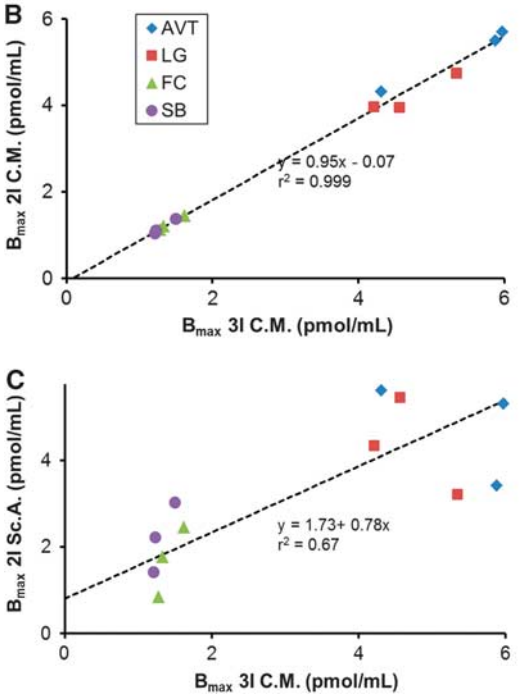

Figure 5. Comparison of B_{max} values, in pmol/mL, estimated with four different analysis methods: compartment modeling of three injections (3I C.M.), compartment modeling of two injections (2I C.M.), three-point Scatchard Plots (3I Sc.A.), and two-point Scatchard plots (2I Sc.A.). Regions examined include the antereoventral thalamus (AVT, ♦), lateral geniculate (LG, ■), frontal cortex (FC, ▲), and subiculum (SB, ●). (**A**) Summarizes the average regional B_{max} values for the different analysis methods. Uncertainty values are based on the standard deviation of the three subjects analyzed (RH1, RH2, and RH3). (**B**) Compares 3I C.M. with 2I C.M. (**C**) Compares 3I C.M. with 2I Sc.A.

detectable 2-[^{18}F]FA specific binding in this region.[11,37] Alternative reference regions, such as the corpus callosum or pons, were not evaluated in this work because of the absence of anatomical MRI data to aid in region identification. In the absence of a valid reference region, modifications to the modeling methods presented herein may be necessary for accurate parameter measurements in human studies. Compartment modeling techniques simultaneously incorporating data from regions of low [^{18}F]nifene uptake with high binding regions may more precisely aid in the identification of a global V_{ND} without an explicit reference region. Alternatively, previous PET and SPECT experiments found that smoking to satiety resulted in $\alpha4\beta2$* nAChR occupancies of 70% to 100%.[36,38] These data suggest the possibility of incorporating a complete displacement dose of nicotine to regionally determine V_{ND} in MI studies.

CONCLUSION

This work presents an *in vivo* measurement of $\alpha4\beta2$* nAChR B_{max} in the rhesus monkey and a first measurement of K_{Dapp} for [^{18}F]nifene using MI techniques. Experiments consisting of two injections in 90 minutes or less precisely identified these parameters, which reduces the experimental complexity from more traditional three-injection designs. Therefore, [^{18}F]nifene enables simplified methods of measuring $\alpha4\beta2$* nAChR B_{max}, allowing for interrogation of this receptor system in disease models and alterations to synaptic levels of acetylcholine because of substance abuse or therapeutic drugs.

DISCLOSURE/CONFLICT OF INTEREST

The authors declare no conflict of interest.

ACKNOWLEDGEMENTS

We thank Professor R Jerry Nickles, Drs Jonathan Engle and Gregory Severin, and Hector Valdovinos for assistance in radioisotope production, Andrew Higgins for contributions with image processing, and Professor Jim Holden for insightful technical discussions. We are grateful to Julie Larson, Leslie Resch, and the staff at the Harlow Center for Biological Psychology (RR000167) for assistance in animal handing and data acquisition.

REFERENCES

1 Perry EK, Lee MLW, Martin-Ruiz CM, Court JA, Volsen SG, Merrit J *et al.* Cholinergic activity in Autism: abnormalities in the cerebral cortex and basal forebrain. *Am J Psychiatry* 2001; **158**: 1058–1066.
2 Burghaus L, Schütz U, Krempel U, Lindstrom J, Schröder H. Loss of nicotinic acetylcholine receptor subunits α4 and α7 in the cerebral cortex of Parkinson patients. *Parkinsonism Relat Dis* 2003; **9**: 243–246.
3 Hellström-Lindahl E, Court JA. Nicotinic acetylcholine receptors during prenatal development and brain pathology in human aging. *Behav Brain Res* 2000; **113**: 159–168.
4 Saricicek A, Esterlis I, Maloney K, Mineur Y, Ruf B, Muralidharan A *et al.* Persistent β2*-nicotinic acetylcholinergic receptor dysfunction in major depressive disorder. *Am J Psychiatry* 2012; **169**: 851–859.
5 Cosgrove KP, Batis J, Bois F, Maciejewski PK, Esterlis I, Kloczynski T *et al.* β2-Nicotinic acetylcholine receptor availability during acute and prolonged abstinence from tobacco smoking. *Arch Gen Psychiatry* 2009; **66**: 666–676.
6 Innis RB, Cunningham VJ, Delforge J, Fujita M, Gjedde A, Gunn RN *et al.* Consensus comenclature for *in vivo* imaging of reversibly binding radioligands. *J Cerebr Blood Flow Metab* 2007; **27**: 1533–1539.
7 Sihver W, Gillberg P, Svensson A, Nordberg A. Autoradiographic comparison of [^{3}H](−)nicotine, [^{3}H]cytisine, and [^{3}H]epibatidine binding in relation to vesicular acetylcholine transport sites in the temporal cortex in Alzheimer's disease. *Neuroscience* 1999; **94**: 685–696.
8 Pimlott SL, Piggott M, Owens J, Greally E, Court JA, Jaros E *et al.* Nicotinic acetylcholine receptor distribution in Alzheimer's disease, dementia with Lewy bodies, Parkinson's disease, and vascular dementia: *in vitro* binding study using 5-[^{125}I]-A-85380. *Neuropsychopharmacology* 2004; **29**: 108–116.
9 Houghtling RA, Davila-Garcia MI, Kellar KJ. Characterization of (±)-[^{3}H]epibatidine binding to nicotinic cholinergic receptors in rat and human brain. *Mol Pharm* 1995; **48**: 280–287.
10 Sihver W, Gillberg P, Nordberg A. Laminar distribution of nicotinic receptor subtypes in human cerebral cortex as determined by [^{3}H](−)nicotine, [^{3}H]cytisine and [^{3}H]epibatidine *in vitro* autoradiography. *Neuroscience* 1998; **85**: 1121–1133.
11 Gallezot J-D, Bottlaender M, Delforge J, Valette H, Saba W, Dollé F *et al.* Quantification of cerebral nicotinic acetylcholine receptors by PET using 2-[^{18}F]fluoro-A-85380 and the multiinjection approach. *J Cerebr Blood Flow Metab* 2008; **28**: 172–189.
12 Pichika R, Easwaramoorthy B, Collins D, Christian BT, Shi B, Narayanan TK *et al.* Nicotinic α4β2 receptor imaging agents: part II. Synthesis and biological evaluation of 2-[^{18}F]fluoro-3-[2-((*S*)-3-pyrrolinyl)methoxy]pyridine (^{18}F-nifene) in rodents and imaging by PET in nonhuman primate. *Nucl Med Biol* 2006; **33**: 295–304.
13 Hillmer AT, Wooten DW, Slesarev MS, Ahlers EO, Barnhart TE, Murali D *et al.* PET imaging of α4β2* nicotinic acetylcholine receptors: quantitative analysis of ^{18}F-nifene kinetics in the nonhuman primate. *J Nucl Med* 2012; **53**: 1471–1480.
14 Hillmer AT, Wooten DW, Moirano JM, Slesarev M, Barnhart TE, Engle JW *et al.* Specific α4β2 nicotinic acetylcholine receptor binding of [F-18]nifene in the rhesus monkey. *Synapse* 2011; **65**: 1309–1318.

15 Salinas C, Muzic RF, Ernsberger P, Saidel GM. Robust experiment design for estimating myocardial β adrenergic receptor concentration using PET. *Med Phys* 2007; **31**: 151–165.
16 Muzic RF, Cornelius S. COMKAT: Compartment model kinetic analysis tool. *J Nucl Med* 2001; **42**: 636–645.
17 Tai YC, Chatziioannou A, Siegel S, Young J, Newport D, Goble RN *et al.* Performance evaluation of the microPET P4: a PET system dedicated to animal imaging. *Phys Med Biol* 2001; **46**: 1856–1862.
18 Feng D, Huang S-C, Wang X. Models for computer simulation studies of input functions for tracer kinetic modeling with positron emission tomography. *Int J Biomed Comput* 1993; **32**: 95–110.
19 Christian BT, Vandehey NT, Floberg JM, Mistretta CA. Dynamic PET denoising with HYPR processing. *J Nucl Med* 2010; **51**: 1147–1154.
20 Delforge J, Syrota A, Mazoyer BM. Identifiability analysis and parameter identification of an *in vivo* ligand–receptor model from PET data. *IEEE Trans Bio Med Eng* 1990; **37**: 653–661.
21 Morris ED, Christian BT, Yoder KK, Muzic RF. Estimation of local receptor density B_{max} and other parameters via multiple-injection PET experiments. In: Abelson JN, Simon MI (eds). *Methods in Enzymology* Vol 385. Academic Press: New York, 2004, pp 184–213.
22 Muzic RF, Christian BT. Evaluation of objective functions for estimation of kinetic parameters. *Med Phys* 2006; **33**: 342–353.
23 Vandehey NT, Moirano JM, Converse AK, Holden JE, Mukherjee J, Murali D *et al.* High-affinity dopamine D2/D3 PET radioligands [^{18}F]-fallypride and [^{11}C]-FLB457: a comparison of kinetics in extrastriatial regions using a multiple-injection protocol. *J Cerebr Blood Flow Metab* 2010; **30**: 994–1007.
24 Farde L, Eriksson L, Blomquist G, Halldin C. Kinetic analysis of ventral [^{11}C]raclopride binding to D2-dopamine receptors studied by PET—a comparison to the equilibrium analysis. *J Cerebr Blood Flow Metab* 1989; **9**: 696–708.
25 Holden JE, Jivan S, Ruth TJ, Doudet DJ. *In vivo* receptor assay with multiple ligand concentrations: an equilibrium approach. *J Cerebr Blood Flow Metab* 2002; **22**: 1132–1141.
26 Lammertsma AA, Bench CJ, Hume SP, Osman S, Gunn K, Brooks DJ *et al.* Comparison of methods for analysis of clinical [^{11}C]raclopride studies. *J Cerebr Blood Flow Metab* 1996; **16**: 42–52.
27 Christian BT, Narayanan T, Shi B, Morris ED, Mantil J, Mukherjee J. Measuring the *in vivo* binding parameters of [^{18}F]-fallypride in monkeys using a PET multiple-injection protocol. *J Cerebr Blood Flow Metab* 2004; **24**: 309–322.
28 Wooten DW, Hillmer AT, Moirano JM, Tudorasacu D, Ahlers EO, Slesarev MS *et al.* 5-HT_{1A} sex based differences in B_{max}, *in vivo* K_D, and BP_{ND} in the nonhuman primate. *NeuroImage* 2013; **77**: 125–132.
29 Josserand V, Pelerin H, De Bruin B, Jego B, Kuhnast B, Hinnen F *et al.* Evaluation of drug penetration into the brain: a double study by *in vivo* imaging with positron emission tomography and using an *in vitro* model of the human blood–brain barrier. *J Pharmacol Exp Ther* 2006; **316**: 79–86.
30 Dischino D, Welch MJ, Kilborun MR, Raichle ME. Relationship between lipophilicity and brain extraction of C-11-labeled radiopharmaceuticals. *J Nucl Med* 1983; **24**: 1030–1038.
31 Allen DD, Lockman PR, Roder KE, Dwoskin LP, Crooks PA. Active transport of high-affinity choline and nicotine analogs into the central nervous system by the blood–brain barrier choline transporter. *J Phramacol Exp Ther* 2003; **304**: 1268–1274.
32 Deuther-Conrad W, Patt JT, Lockman PR, Allen DD, Patt M, Schildan A *et al.* Norchloro-fluoro-homoepibatidine (NCFHEB)—a promising radioligand for neuroimaging nicotinic acetylcholine receptors with PET. *Eur Neuropsychopharmacol* 2008; **18**: 222–229.
33 Hillmer AT, Wooten DW, Farhoud M, Barnhart TE, Mukherjee J, Christian BT. The effects of lobeline on $\alpha4\beta2$* nicotinic acetylcholine receptor binding and uptake of [^{18}F]nifene in rats. *J Neurosci Methods* 2013; **214**: 163–169.
34 Gotti C, Clementi F. Neuronal nicotinic receptors: from structure to pathology. *Prog Neurobiol* 2004; **74**: 363–396.
35 Morris ED, Bonab AA, Alpert NM, Fischman AJ, Madras BK, Christian BT. Concentration of dopamine transporters: to B_{max} or not to B_{max}? *Synapse* 1999; **32**: 136–140.
36 Brody AL, Mandelkern MA, London ED, Olmstead RE, Farahi J, Scheibal D *et al.* Cigarette smoking saturates brain $\alpha4\beta2$ nicotinic acetylcholine receptors. *Arch Gen Psychiatry* 2006; **63**: 907–915.
37 Gallezot J-D, Bottlaender M, Gregoire M-C, Roumenov D, Deverre J-R, Coulon C *et al.* *In vivo* imaging of human cerebral nicotinic acetylcholine receptors with 2-[^{18}F]-Fluoro-A-85380 and PET. *J Nucl Med* 2005; **46**: 240–247.
38 Esterlis I, Cosgrove KP, Batis JC, Bois F, Stiklus SM, Perkins E *et al.* Quantification of smoking-induced occupancy of β2-nicotinic acetylcholine receptors: estimation of nondisplaceable binding. *J Nucl Med* 2010; **51**: 1226–1233.